# In-situ 3D observation of hydrogen-assisted particle damage behavior in 7075 Al alloy by synchrotron X-ray tomography

Wang, Yafei
Department of Mechanical Engineering, Kyushu University

Toda, Hiroyuki
Department of Mechanical Engineering, Kyushu University

Xu, Yuantao
Department of Mechanical Engineering, Kyushu University

Shimizu, Kazuyuki
Department of Physical Science and Materials Engineering, Iwate University

他



出版情報：Acta materialia. 227, pp.117658-, 2022-04-01. Elsevier
バージョン：
権利関係：

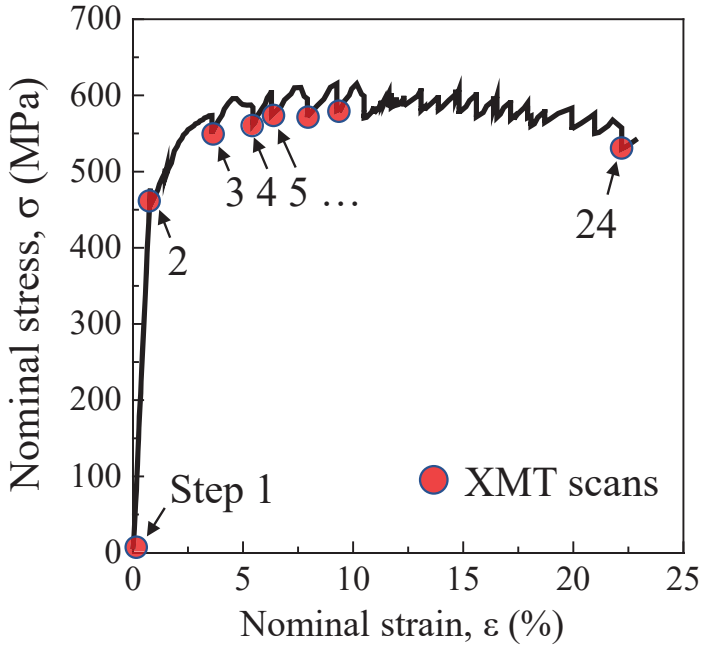


**Fig. 1.** Nominal stress-strain curve obtained from an *in-situ* tensile test with a small strain increment.

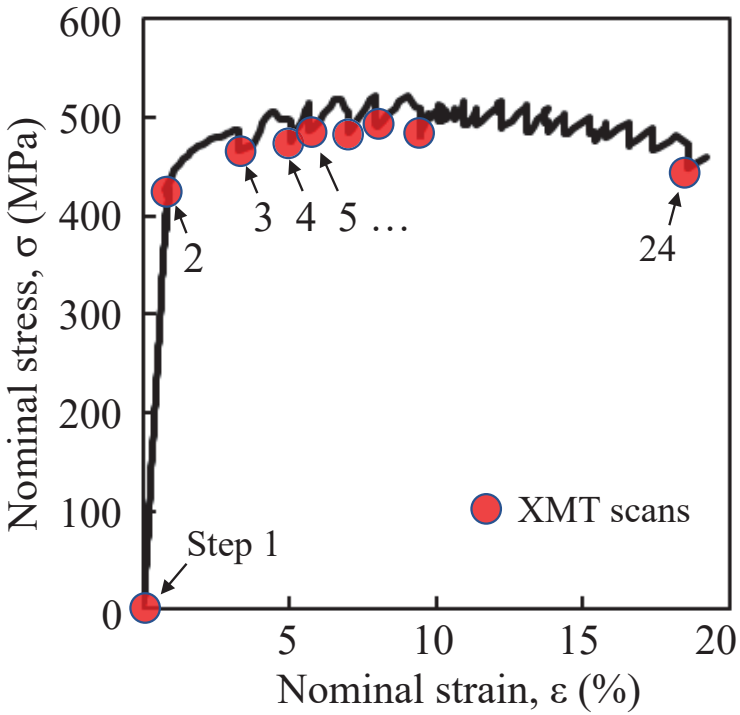


**Fig. 1.** Nominal stress-strain curve obtained from an *in-situ* tensile test with a small strain increment.

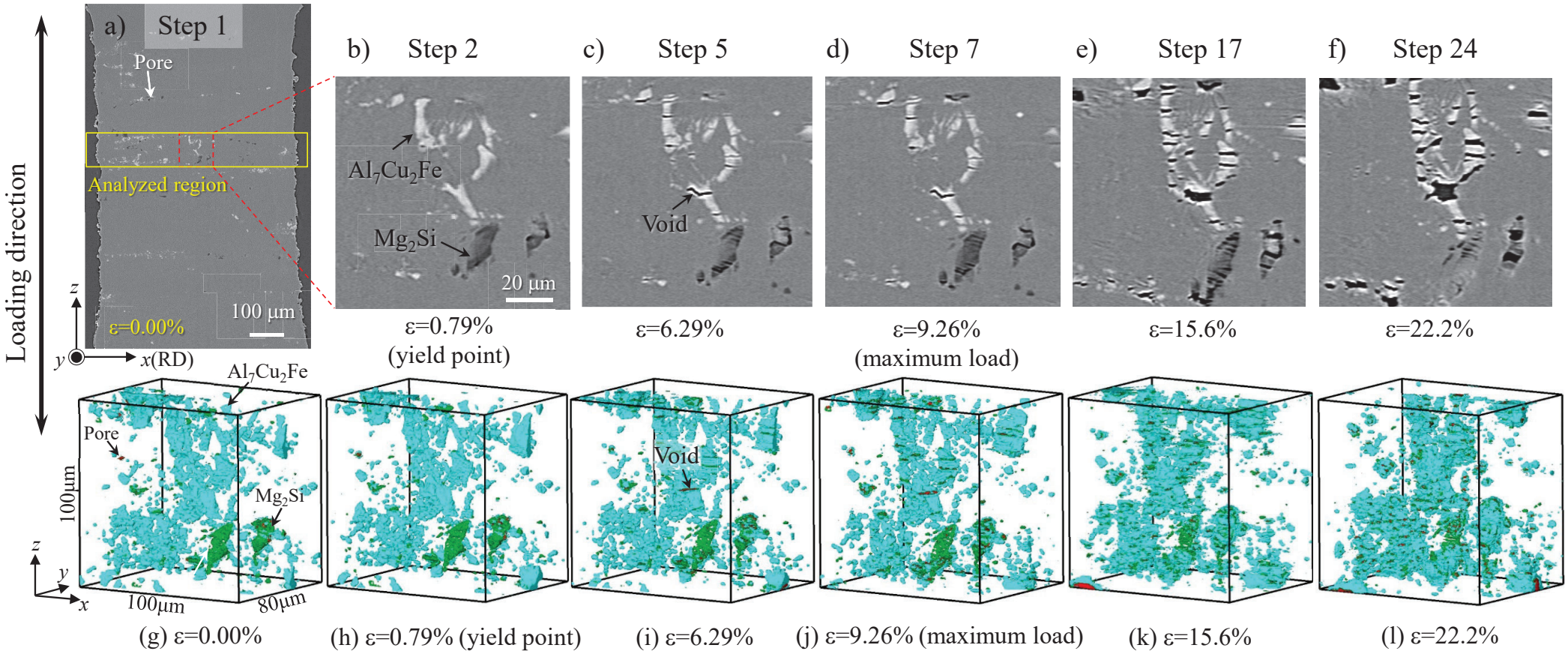


**Fig. 2**. Virtual cross sections in the *x*-*z* plane captured by XMT at (a) ε=0.00%, (b) ε=0.79% (yield point), (c) ε=6.29%, (d) ε=9.26% (maximum load), (e) ε=15.6%, and (f) ε=20.0%. The corresponding 3D perspective views at different applied strains, for the region indicated by the red dashed line in (a), are shown from (g) to (l). The yellow solid line in (a) indicates the region for particle damage analysis.

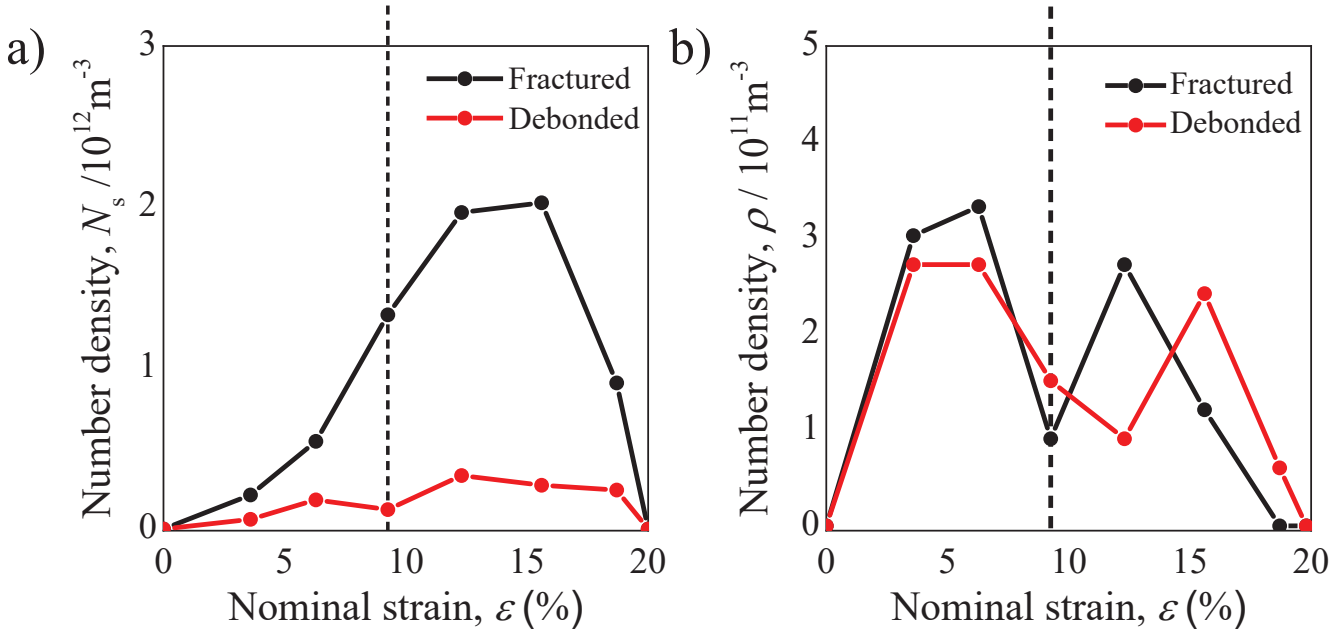


**Fig. 3**. Number density of fractured and debonded (a) $Al_7Cu_2Fe$ and (b) $Mg_2Si$ particles at different applied strains. The maximum load point is shown as a black dotted line.

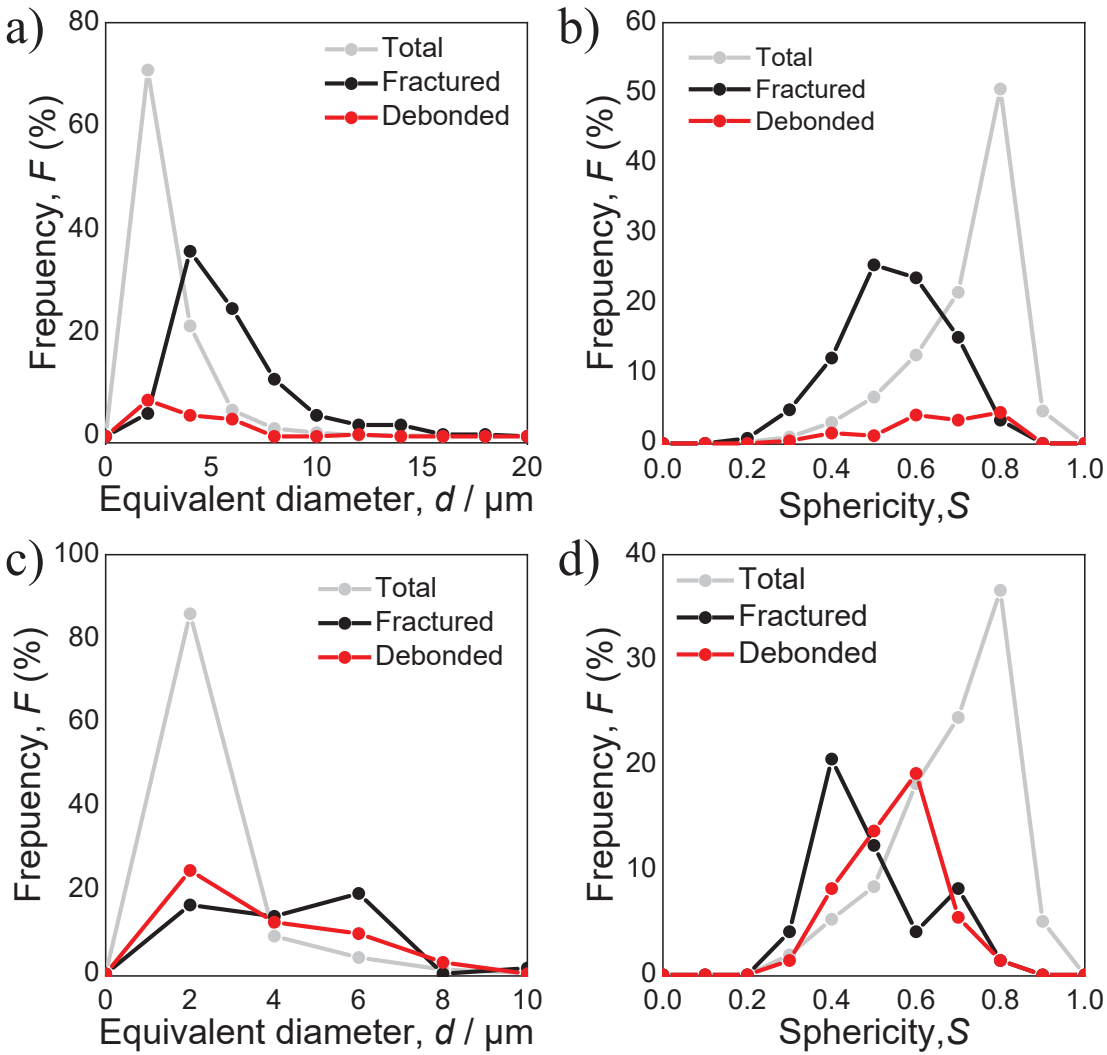


**Fig. 4**. Frequency distributions as a function of equivalent diameter and sphericity for (a), (b) $Al_7Cu_2Fe$ and (c), (d) $Mg_2Si$ particles.

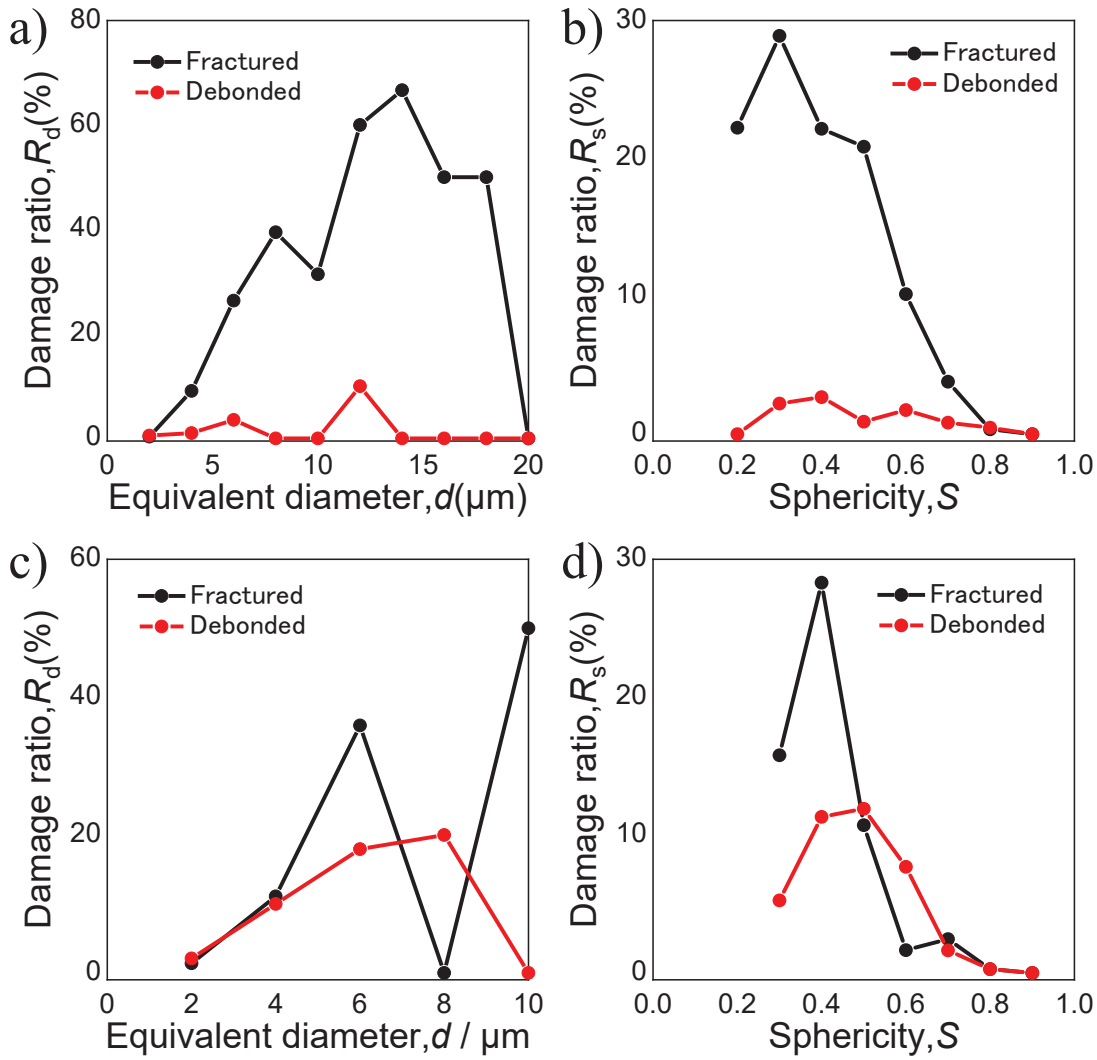


**Fig. 5.** Damage ratios as a function of equivalent diameter or sphericity for (a), (b) $Al_7Cu_2Fe$ particles and (c), (d) $Mg_2Si$ particles.

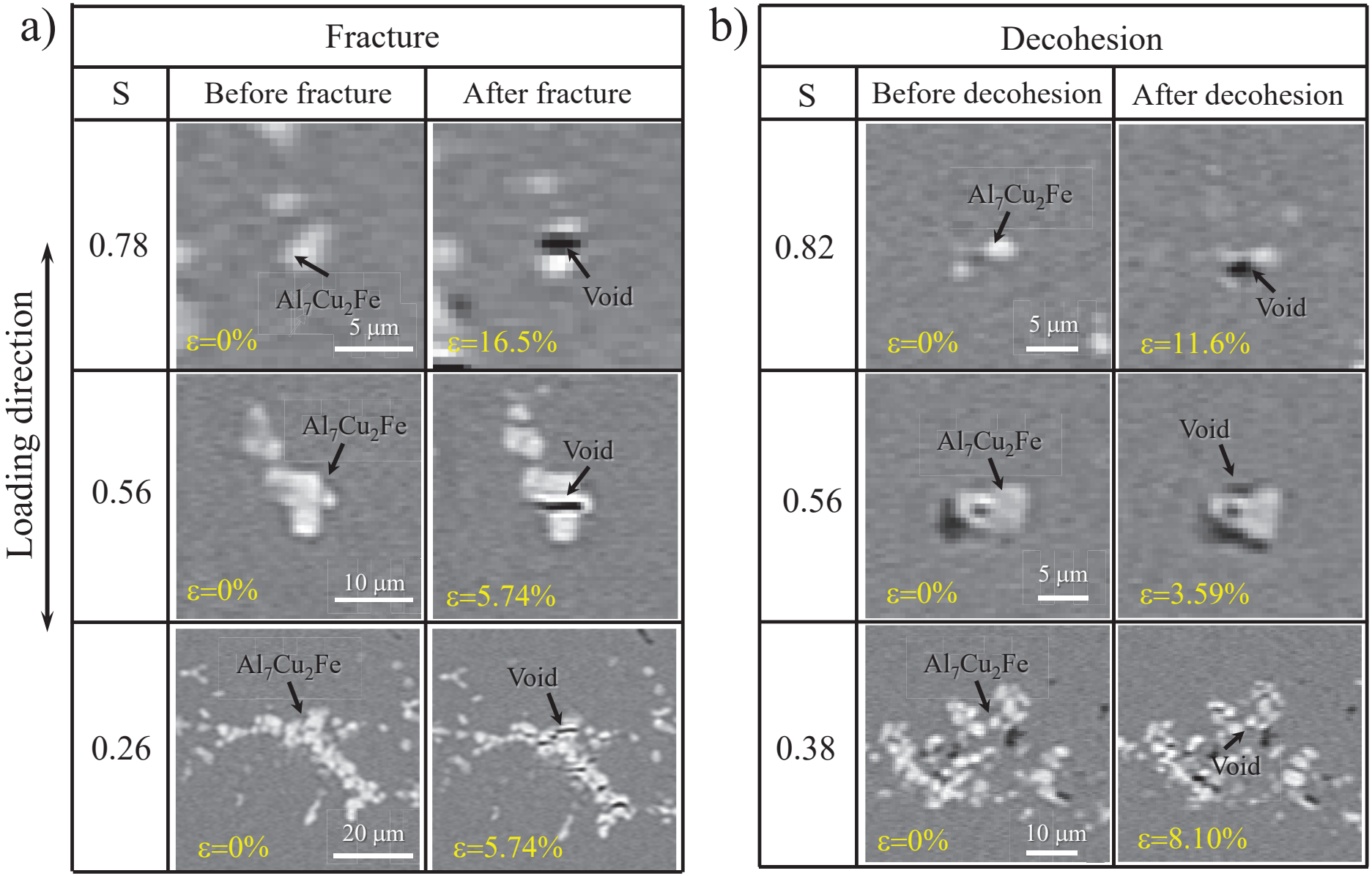


**Fig. 6.** Morphologies of $Al_7Cu_2Fe$ particles with different sphericities, *S*, before and after (a) fracture and (b) debonding.

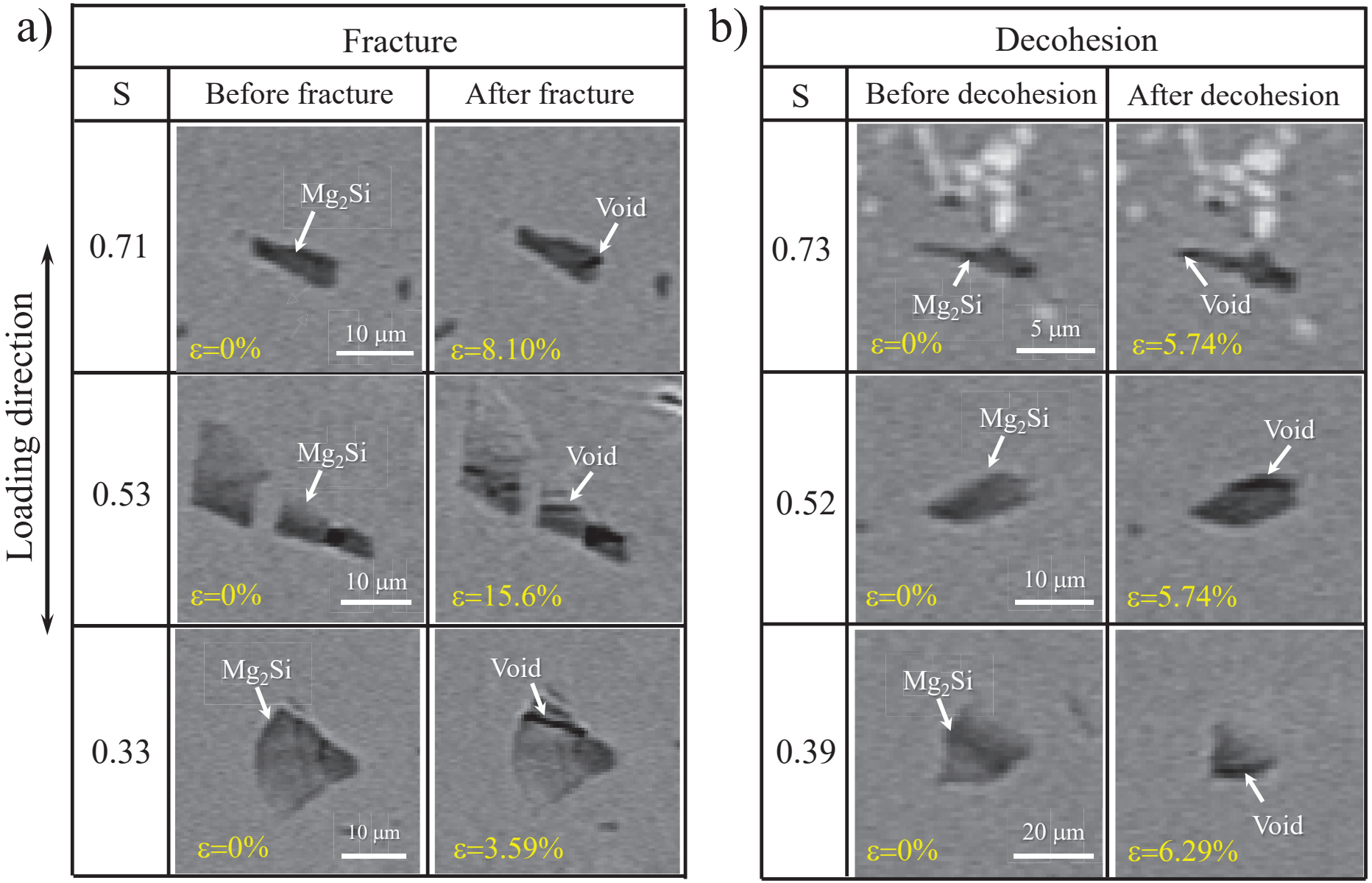


**Fig. 7.** Morphologies of $Mg_2Si$ particles with different sphericities, *S*, before and after (a) fracture and (b) debonding.

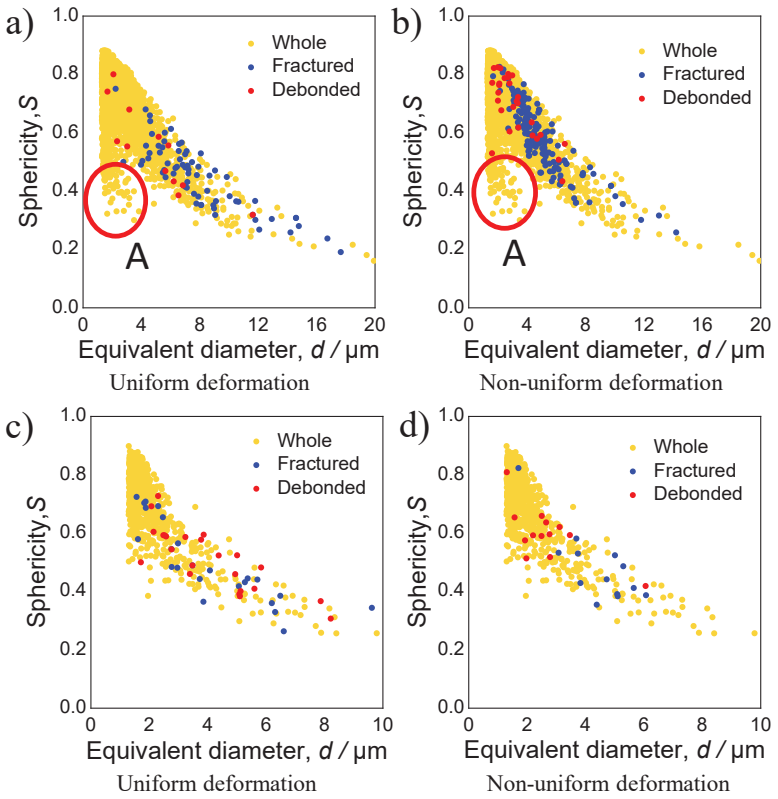


**Fig. 8.** Relationship between equivalent diameter and sphericity in (a), (b) $Al_7Cu_2Fe$ particles and (c), (d) $Mg_2Si$ particles in the necking region. Yellow dots indicate all particles, while fractured and debonded particles are shown in blue and red, respectively. (a) and (c) show data for uniform deformation, while (b) and (d) show data for nonuniform deformation. The yellow dots indicated by 'A' are artefacts.

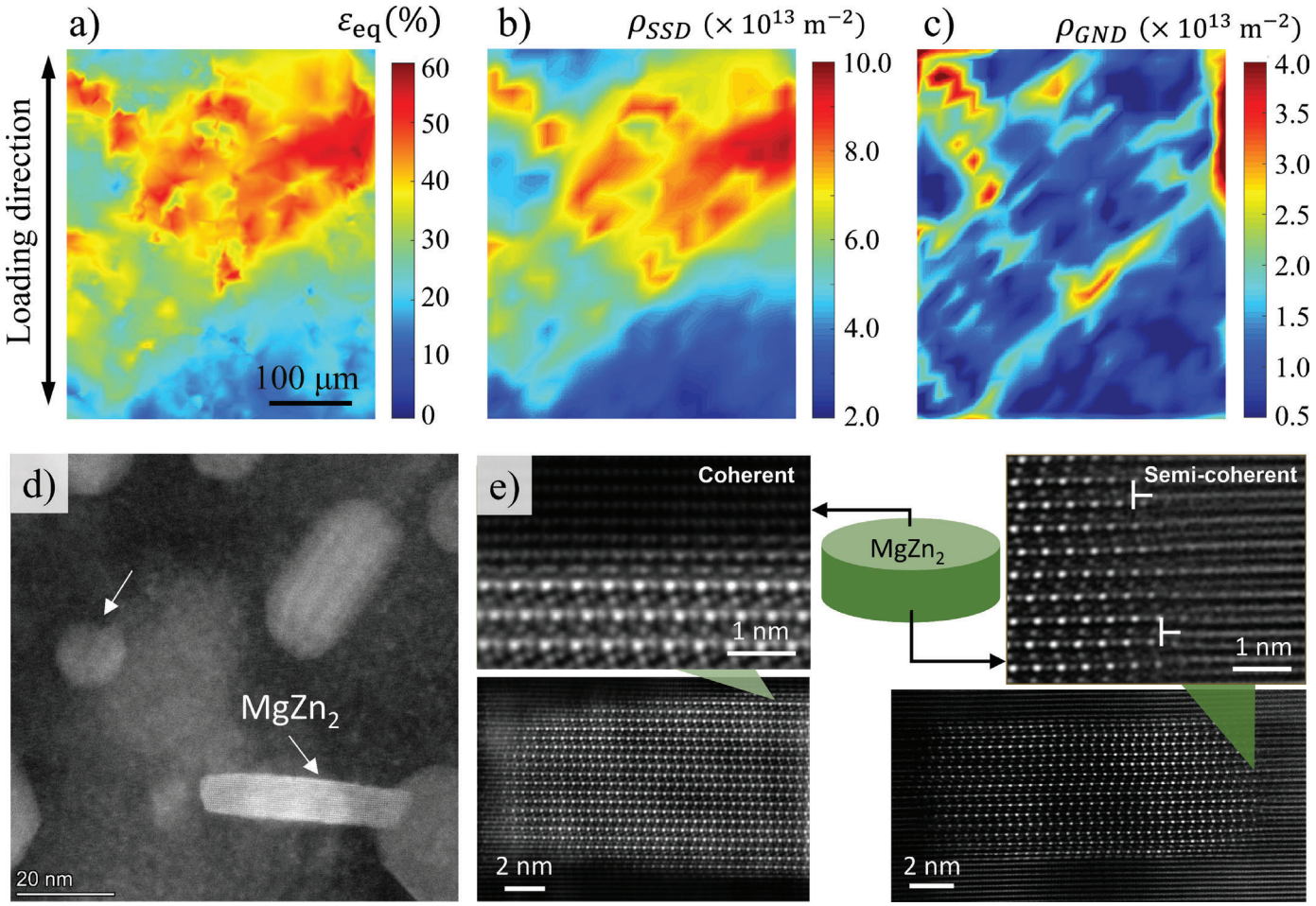
a)
$\varepsilon_{eq}$(%)
Loading direction
100 μm
60
50
40
30
20
10
0
b)
$\rho_{SSD}$ (× $10^{13}$ $m^{-2}$)
10.0
8.0
6.0
4.0
2.0
c)
$\rho_{GND}$ (× $10^{13}$ $m^{-2}$)
4.0
3.5
3.0
2.5
2.0
1.5
1.0
0.5
d)
$MgZn_2$
20 nm
e)
Coherent
1 nm
2 nm
$MgZn_2$
Semi-coherent
1 nm
2 nm

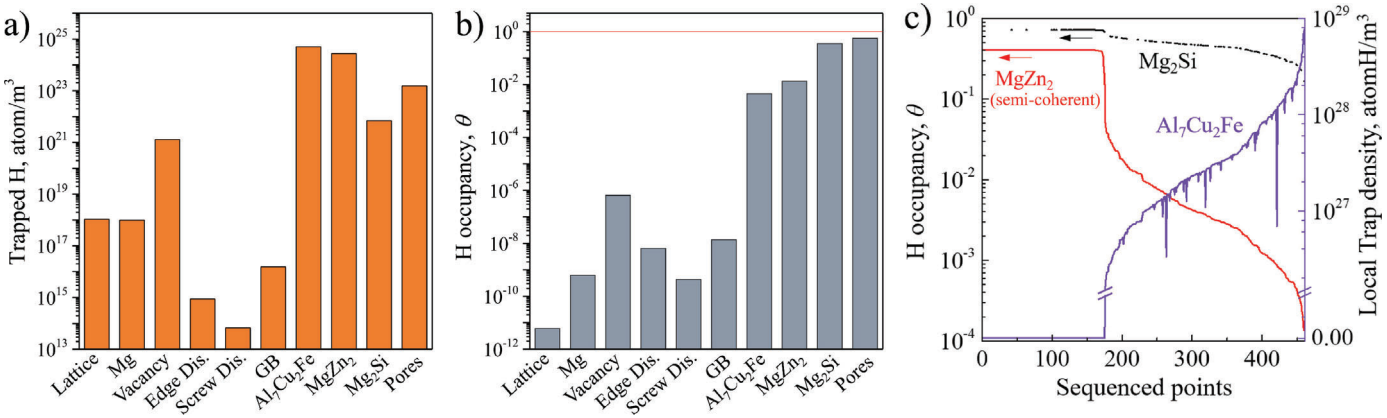
a)
Trapped H, atom/m3
Lattice
Mg
Vacancy
Edge Dis.
Screw Dis.
GB
Al7Cu2Fe
MgZn2
Mg2Si
Pores
b)
H occupancy, θ
c)
MgZn2
(semi-coherent)
Mg2Si
Al7Cu2Fe
Local Trap density, atomH/m3
Sequenced points

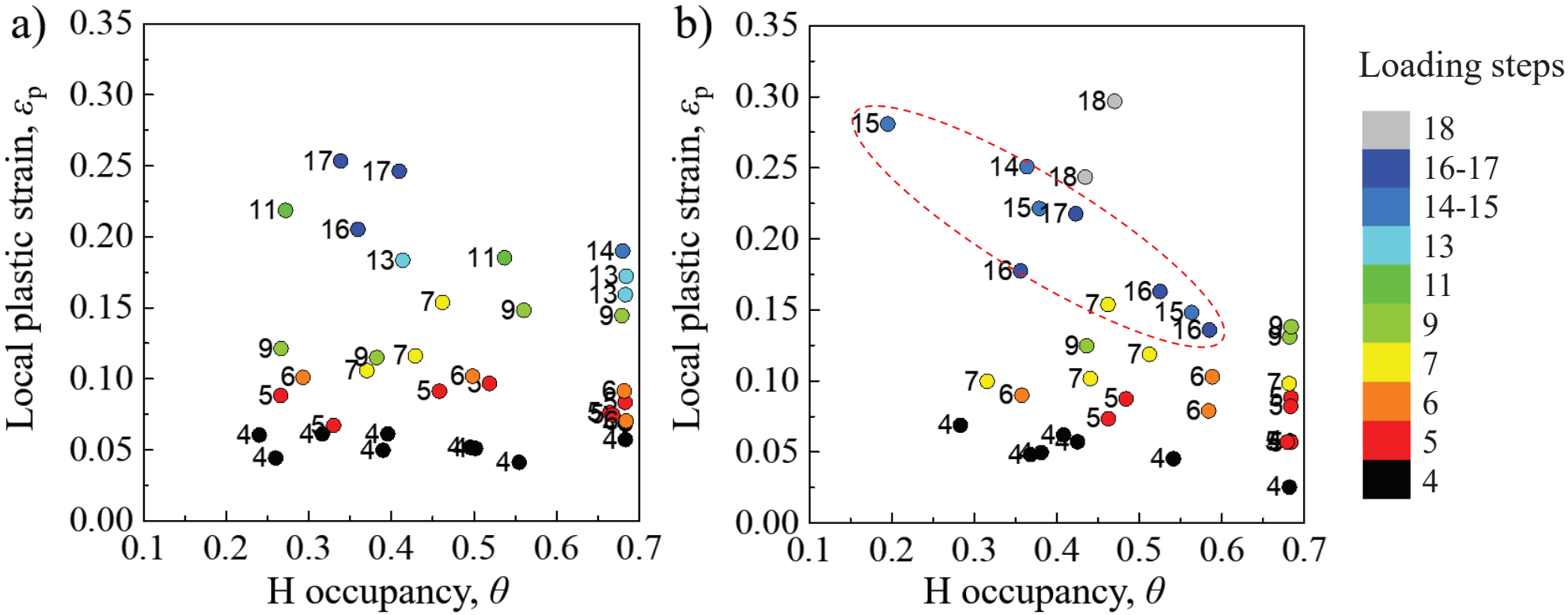


**Fig. 11**. Local plastic strain and hydrogen occupancy at (a) fractured and (b) debonded $Mg_2Si$ particles. The color codes and the numbers indicate the different loading steps in which particle damage occurs.

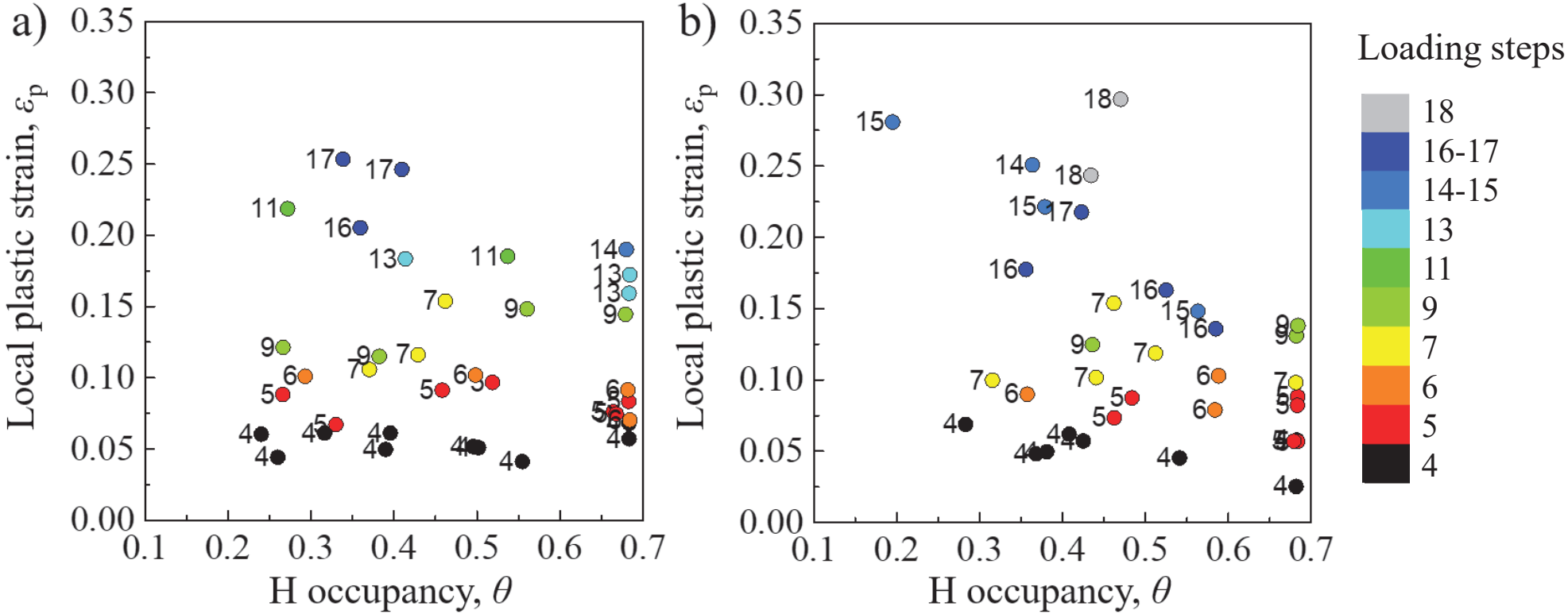


**Fig. 11**. Local plastic strain and hydrogen occupancy at (a) fractured and (b) debonded $Mg_2Si$ particles. The color codes and the numbers indicate the different loading steps in which particle damage occurs.